

High-Speed Video of Metal Transfer in Submerged Arc Welding

Metal transfer in SAW is presented in high-quality, high-speed video

BY P. F. MENDEZ, G. GOETT, AND S. D. GUEST

ABSTRACT

Metal transfer in submerged arc welding (SAW) has been captured in video at a rate of 10,000 frames per second by inserting a thin-gauge steel tunnel along the welding path. Precedents in the scientific literature for high-speed imaging of metal transfer in SAW are almost 40 years old using photographic film at speeds of 3000 frames per second or below. Analysis of the new videos show that at 500 A, a very chaotic, nonaxial globular metal transfer involving frequent explosions and bursts is present in both AC and DC polarities. A droplet detachment frequency of approximately 9 Hz was observed at 500-A DCEP, and 13 Hz at 500-A AC. At 1000-A DCEP, a tapering electrode tip with a buried arc was observed ejecting a molten tail through a mechanism resembling an electromagnetic kink instability. Analysis of the voltage signal indicates a $1/f$ pink noise without any indication of the events observed in the videos. Spectrometry of the arc in the weld cavity was performed, and no obvious signs of external gas entrainment were detected. Analysis of the weld cross sections show a significant increase in penetration at 1000 A, consistent with the gouging region penetration mode observed in the videos. The technique presented here opens the door for high-speed video analysis of metal transfer and the design of complex waveforms in SAW.

KEYWORDS

- Submerged Arc Welding (SAW) • High-Speed Video • Metal Transfer
- Spectroscopy

Introduction

The mode of metal transfer in arc welding is crucial to the quality of the weldment. Experience from gas metal arc welding (GMAW) shows the metal transfer mode affects weld penetration, weld width, recovery of alloying elements, fume emission, spatter, wetting, and more (Ref. 1). Because the arc is submerged under fluxes, the mode of metal transfer in submerged arc welding (SAW) is not directly ob-

servable. This ignorance of the mode of metal transfer may have limited the development of welding equipment. Modern SAW hardware is capable of handling waveforms of high complexity, but in the absence of understanding this potential cannot be realized. Computer models of SAW such as in Refs. 2 and 3 rely on best guesses about the mode of metal transfer and how it affects the heat transfer and fluid mechanics of the weld bead, but lack experimental verification.

The earliest attempts at imaging metal transfer in SAW were based on X-ray radiography, among them Refs. 4–6. The earliest published attempt at optical high-speed videography of metal transfer in SAW is by Tybus in Germany in 1957 (Ref. 7) using a glass plate on the sagittal plane of the weld through which the flux cavity could be filmed. Videos produced by Tybus had a frame rate of 750 frames per second (f/s) and low resolution for current standards.

In 1965, Franz used a ceramic tube that penetrated the fluxes with its axis parallel to the direction of welding and photographic film at a speed of 3000 f/s (Ref. 8) and with much better resolution than Tybus. Franz injected gas (Ar and CO₂) into the weld cavity with the stated goal of preventing its collapse. The conditions tested were similar to those tested in this work; for example, the run of Table 21 of Ref. 8 was done at a current between 500 and 510 A, voltage between 31 and 33 V, wire feed speed of 1.62 m/min, and wire diameter of 3 mm, all very similar to Experiment 5 presented here. Franz used a travel velocity of 0.2 cm/s, roughly half of what was used in this work; a possible reason for the choice of this slow speed is that the weld travel was toward the camera and faster travel speed would have resulted in a very short time interval in which to create a good set of images.

Lancaster (Ref. 9) mentions that Van Adrichem also used a setup similar to Franz's in 1966 (Ref. 10). Franz's

P. F. MENDEZ (pmendez@ualberta.ca) is with Canadian Centre for Welding and Joining, University of Alberta, Edmonton, AB, Canada. G. GOETT is with INP Greifswald, Germany. S. D. GUEST is with Stantec, Inc., Calgary, AB, Canada.

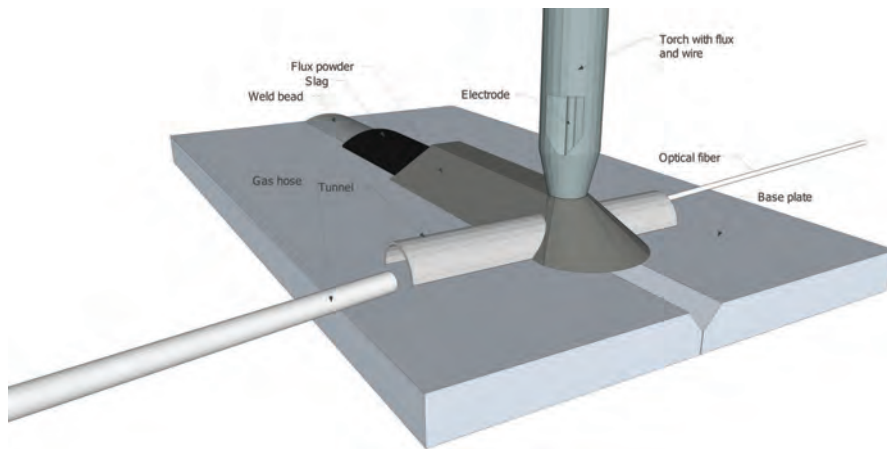


Fig. 1 — Experimental arrangement to create high-speed videos of metal transfer in SAW.

technique was also used by Gupta et al. (Ref. 11) in 1976 to study the influence of pulsing in SAW with a frame rate of 1800 to 2200 f/s. This reference is the last published attempt at high-speed videography of metal transfer in SAW until recently. The images of Refs. 8 and 11 were a significant accomplishment that was never reproduced in the literature until Ref. 12. Current research on imaging of metal transfer in SAW includes the excellent work by Reisingen et al. (Ref. 13) where all previous SAW imaging techniques are tested and compared.

In the work presented here, metal transfer in SAW has been captured in video at a rate of 10,000 f/s. The image quality and frame rate of the new images is far superior to previous attempts because of the use of modern equipment and an improved setup of the experiment. The new videos were first shown at Ref. 12, and are uploaded at Ref. 14 as supporting online material (SOM).

Experimental Setup

The new technique developed is illustrated in Fig. 1. The key element is a “tunnel” across the welding path that

is placed before the welding operation. The direction of the tunnel is perpendicular to the direction of welding, such that the weld will cut across the tunnel. The tunnel is made of steel sheet that was sanded and cleaned to remove all traces of zinc coating, and then rolled to a thickness of approximately 0.5 mm. The tunnel has an approximately semicircular cross section with a radius of 6 to 10 mm. The top of the tunnel was always completely covered by flux powders.

The choice of steel for the tunnel material was for facilitating construction and to cause minimum disruption of the weld. Glass tunnels were also tried but did not melt fast enough and the wire mechanically pushed them aside; steel tunnels caused occasional stray arcs above the molten droplet, these stray arcs cut a path across the tunnel without mechanical interference. Previous attempts by the authors to image SAW using quartz rods were unsuccessful, as the end of the rod exposed to the weld would get dirty and block the line of sight of the camera. A tunnel perpendicular to the direction of welding was chosen over a longitudinal arrangement to avoid long amounts of ejected debris blocking the

view and also to achieve better focus.

The camera was trained into the weld from one end of the tunnel. A flow of gas was injected from the same side of the camera view; the function of this gas was to blow away stray flux particles that blocked the camera view when the wire started cutting across the tunnel. Our preliminary evidence suggests the effect of this gas is minimal once the electrode is fully into the tunnel. In the opposite end of the tunnel, an optic fiber was positioned, connected to a spectrometer that was used to identify the presence of external gases in the weld cavity.

The welding power supply used was a Lincoln AC/DC 1000 (WeldSet Name Z123334) running Powerwave Manager 1.0.2.5. The welds were performed as “bead on plate” without weaving (straight stringer beads) with a contact tip-to-workpiece distance of 1.25 in. (31.8 mm) and a constant travel speed. The wire used was Lincolnweld L-50, diameter 0.125 in. (3.2 mm), and the flux used was Lincolnweld 980 with a basicity index of 0.6 (EM13K and F7A2, respectively, in AWS A5.17). All DC experiments were performed with Program No. 58 (CC DC+ Steel 0.125 in.). All AC experiments were performed using Program No. 59 (CC Square Wave Steel 0.125 in.) with a frequency of 50 Hz and a balance of 75% electrode positive (EP) and 25% electrode negative (EN). The offset was such that the target voltage was kept constant during both EP and EN polarities. Data acquisition of current, voltage, and wire feed speed was performed at 60 kHz using the embedded electronics of the power supply and ArLink software (PT-WT-WS-GT-MD 6-2-15-0-18154499).

The high-speed camera used was a Phantom V210 at a frame rate of 10,000 f/s and resolution of 512 by 360 pixels (videos SOM2, SOM3, SOM4) or 9300 f/s and resolution of 624 by 360 pixels (video SOM6). A

Table 1 — Parameters of Experiments Corresponding to Uploaded Videos

Experiment	Video	Target Current	Target Voltage	Polarity	Average WFS		Travel speed		Gas for tunnel
		A	V		m/min	in./min	m/min	in./min	
5	SOM2	500	30	DCEP	1.61	63.4	0.457	18	CO ₂
12	SOM1, SOM3	500	30	AC	1.79	70.5	0.457	18	CO ₂
10	SOM4	1000	38	DCEP	4.47	176.0	0.711	28	CO ₂
15	SOM6	500	30	DCEP	1.57	61.8	0.457	18	Ne

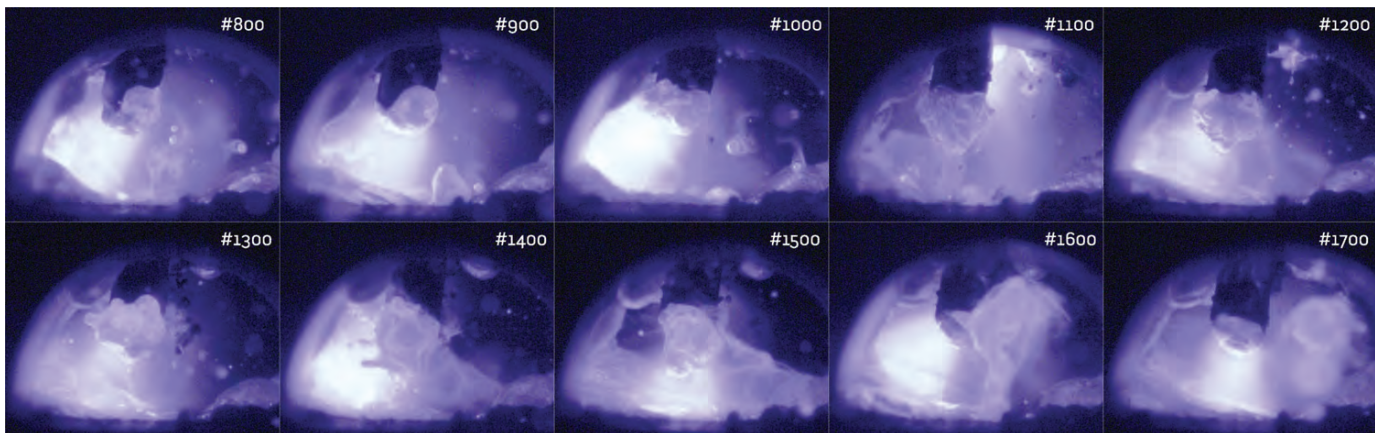


Fig. 2 — Metal transfer in SAW during Experiment 5 (500-A, 30-V DCEP). This figure shows frames 800 to 1700 at 100-frame intervals (total time elapsed is 0.09 s). There is a detachment event between frames 1600 and 1700. For a sense of scale, consider that the wire diameter is 0.125 in. (3.2 mm).

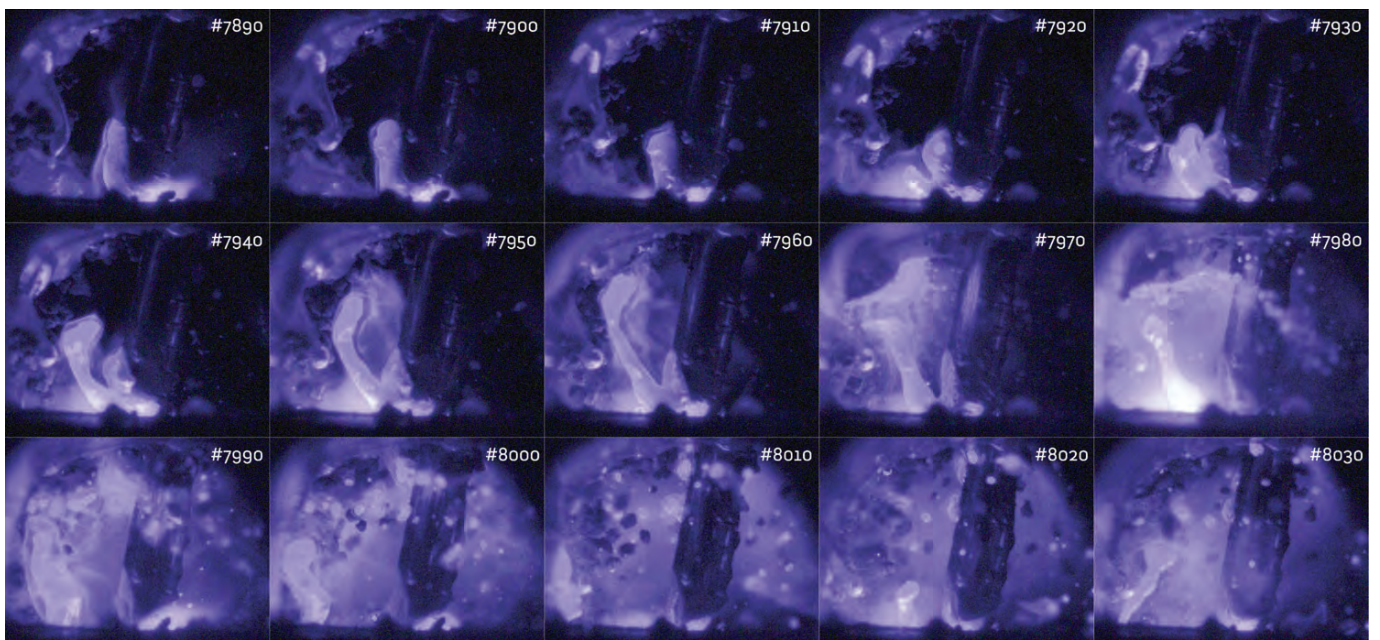


Fig. 3 — Metal transfer in SAW during Experiment 10 (1000-A, 38-V DCEP). This figure shows frames 7890 to 8030 at 10-frame intervals (total time elapsed is 0.014 s). The arc is "buried," and there is metal ejection resembling a kink instability. For a sense of scale, consider that the wire diameter (visible in frame 8000) is 0.125 in. (3.2 mm).

180-mm lens was used with extension tubes to accomplish the desired magnification, and a single 850-nm-long pass filter was used. Correct focus on the wire was reached before placement of the base plate, but with the filter in place. Spectra were collected using an Ocean Optics HR4000CG spectrometer. The video, electrical signal, and gun position were not synchronized, but they can be approximately related to each other through identifiable simultaneous features that appear in more than one data stream.

The operation of the experiment is illustrated in the video SOM1, corre-

sponding to Experiment 12 (500 A, AC). This video shows the gun approaching and cutting across the tunnel. The green hose on the left created a strong flow of gas that was not quantified; however, the maximum flow rate for the regulator used was 40 ft³/h for CO₂ (a representative gas flow rate for GMAW is 35 ft³/h). The optic fiber with a blue sheath is seen on the right; it was withdrawn immediately after the spectrum was taken to avoid excessive damage of the fiber by the ejected debris. When the electrode reaches the tunnel, a strong flow of gas and sparks is seen coming out of both ends of the tunnel

without a visible bias due to the gas blown by the hose.

High-Speed Videos

Four high-speed videos of metal transfer in SAW are uploaded as supporting online material (Ref. 14), and their welding parameters are listed in Table 1. The videos are rendered at 30 f/s, which corresponds to a factor of 333 in the time dimension for videos SOM2, SOM3, and SOM4. The process parameters used are typical of SAW operation. Many more than the exper-

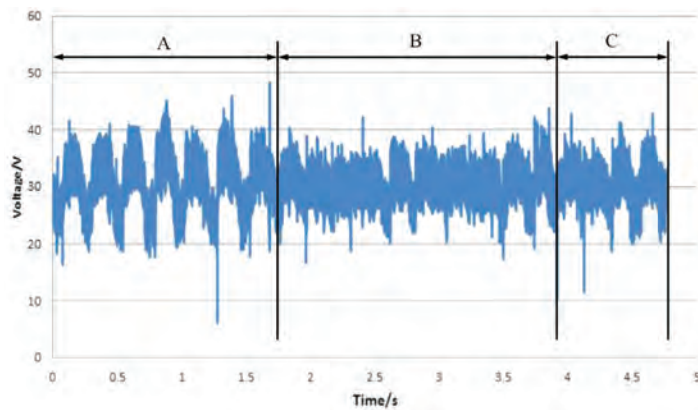


Fig. 4 — Voltage signal of Experiment 5.

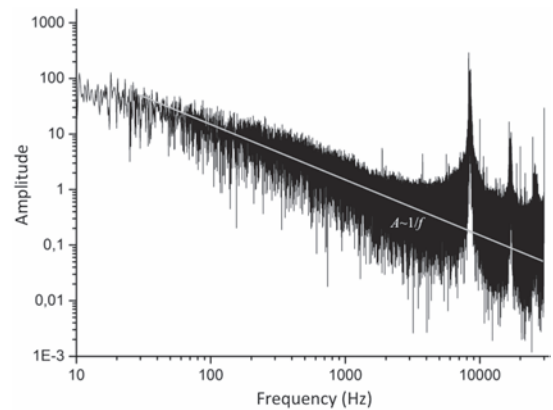


Fig. 5 — FFT analysis of whole voltage signal of Experiment 5.

iments discussed here were attempted, not all of them yielding good videos, and some experiments explored parameters to be discussed in separate publications.

Video SOM2 corresponds to Experiment 5 (500 A, DCEP), and Fig. 2 summarizes frames 800 to 1800 at 100-frame intervals. From the first frame of the video onward, it can be seen that the mode of metal transfer is free flight, as it is also appreciated in Fig. 2. A visual count of the number of “droplet” detachments yields an approximate frequency of detachment of 9 Hz, based on a count of eight detachments, approximately at frames 625, 1613, 3203, 3928, 5700, 6608, 8400, and 9415. The evolution leading to detachment around frame 1613 is captured in Fig. 2. Based on the measured wire feed speed and detachment frequency, the approximate spherical droplet size would be 3.6 mm diameter, ruling out a spray transfer mode for these conditions and metal transfer in this case could be thought of as a form of globular transfer.

Video SOM2 also shows the shape of the droplet is very irregular and much more complex than the globular droplets seen in GMAW; this is consistent with a reduced effect of capillary forces at the large droplet sizes at play. The video also shows frequent explosions in the melt (for example in frame 85), and spatter, adding to the chaotic behavior of the metal transfer. Similar molten metal explosions were reported by Gupta (Ref. 11). The frequency of spatter, explosions, and other perturbations is faster than the natural frequency of oscillation of a detached

droplet of 3.6 mm diameter (such droplet would have a first mode of oscillation at approximately 86 Hz). There is some degree of uncertainty when attempting to identify “droplet” detachments. The large fluctuations in the molten tip of the electrode are of the same order of the droplet diameter, and the attachment of the arc to the electrode and weld pool is erratic. This is consistent with the fact that signal analysis of metal transfer in SAW seldom yields a clear dominant frequency of metal transfer, in stark contrast with gas metal arc welding (GMAW) where droplet detachment events can typically be well identified in globular, pulse, and short circuit transfer modes.

Because the steel tunnel was in electrical contact with the base plate, on occasion, the arc occurred between the electrode and the tunnel (see frame 1055). In this case, it can be seen how the arc at the tip of the electrode is extinguished simultaneously with the appearance of an arc between the electrode and the tunnel (at top of the image). This secondary arc is undesirable, but lasts briefly (approximately 60 frames, or 6 ms); future experiments might be able to use a thin material and a tunnel geometry that melts with the heat from the arc before it establishes contact with the electrode. This video also shows the granules of flux powder falling from the broken top of the tunnel (frame 1275).

Video SOM3 corresponds to Experiment 12 and was run in the same conditions as Experiment 5, but with AC polarity instead of DCEP. For the wave-

form and video parameters used, the EP period lasts 150 frames (5 s in the rendered video), and the EN period lasts 50 frames (1.7 s in rendered video). The effects of switching polarity can be seen when they are not masked by other artifacts in the chaotic metal transfer process. Frame 2369 shows the start of an EN cycle, which lasts until the switch to EP around frame 2415. Polarity reverses to EN around frame 2571, and back to EP in frame 2622. Frames 2582–2620 (during an EN cycle) capture a cathode spot, which looks like a very bright area at the bottom left surface of the droplet. After starting, this cathode spot moves higher and to the right, pushing and deforming the droplet as it moves. Many of the same features observed in Video SOM2 are present. A count of detachments around frames 731, 1404, 2015, 2853, and 3778 suggests an approximate detachment frequency of 13 Hz, and a spherical droplet diameter of approximately 3.3 mm.

Video SOM4 corresponds to Experiment 10, and Fig. 3 summarizes frames 7890 to 8030 at 10-frame intervals. Experiment 10 was run in the same conditions as Experiment 5, but with a target current of 1000 A. The most important feature of this video is that the arc is “buried,” meaning the weld pool surface is so depressed that the arc happens almost completely out of sight below the original surface of the workpiece. The video starts showing how the tunnel is penetrated by the electrode, and Frames 6200 to 7500 show how the electrode buries after crossing the tunnel wall. The mode of metal transfer seems to be unstable and based on the electromag-

Table 2 — Measurements of Cross Sections of Figs. 7 and Fig. 8. (Accuracy of measurement is of the order of 0.1 mm.)

Experiment	Location relative to tunnel	Thickness of plate mm	Bead width mm	Penetration mm	Reinforcement mm
5 (500 A, DC)	before	9.441	16.64	5.54	2.64
	during	9.449	16.94	4.15	3.42
	after	9.442	17.68	6.35	1.89
12 (500 A, AC)	before	9.463	16.86	4.39	2.84
	during	9.452	20.40	3.54	4.88
	after	9.454	16.35	5.05	1.91
10 (1000 A, DC)	before	18.857	11.18	14.17	5.70
15 (500 A, DC, Ne)	before	9.444	16.42	5.91	2.85
	during	9.448	20.34	4.94	4.00
	after	9.428	15.85	6.09	1.84

netic kink instability, somewhat similar to rotating transfer, except that in this video the kink does not seem to rotate.

Frames 7546 to 7888 (approximately) show a fluid bridging the electrode and the weld pool. No sudden arc perturbations are seen when the fluid bridges the electrode and the weld pool, and data acquisition of voltage did not show short circuit events, so it is likely that this fluid is slag. Frame 7646 shows an arcing event on the roof of the tunnel. Frames 7766–7912 show the arc between the electrode and the bottom of the weld pool. Only the top part of the arc is seen, and the rest is below the line of sight. Frames 7912–8010 show an episode of ejection of molten metal in the form of a kink instability. Metal flies sideways and upward at high speeds, and it is likely to hit the wall of the molten flux cavity and drip down its side, eventually joining the weld pool.

Frame 7649 clearly shows the indentations caused in the wire by the knurled rollers in the feeding system. There has been some amount of informal debate in the welding community about the possibility of spray transfer in SAW. There is no evidence of spray transfer in any of the experiments performed, but at 1000 A the electrode tapers in a similar way to that observed in streaming spray transfer (no steady stream of small droplets was observed, just ejections with kink instability). A good example of tapering and detachment is in Frame 8870, when tapering starts, followed by a strong longitudinal flow along the taper in frames 8922 to 9549, finally

ejecting a kinked tail of molten electrode in frame 9641.

Electrical Signal

Spreadsheet SOM5 contains the raw data acquisition of voltage, current, and wire feed speed of the experiments discussed here. In the experiments performed, typically there is no obvious indication of a difference between signal before, during, and after the tunnel.

Experiment 5 is one of those that did show a difference in voltage trace, illustrated in Fig. 4. The 4.8 s of data collected correspond to 36.6 mm of gun travel. The data show three distinct regions, labeled A, B, and C. Although data acquisition and position were not synchronized, based on the start and stop times for data acquisition and the size of the tunnel, it is reasonable to assume these three regions correspond to before, during, and after the tunnel, respectively.

Regions A and C look similar, noisy with a dominant frequency of approximately 4.7 Hz; this dominant frequency relates to variations in wire feed speed as the power supply controls wire feed speed to stay on the target current and voltage. Region B lasts approximately 2.2 s (18 mm) and shows noise without a dominant low frequency.

Figure 5 shows the Fast Fourier Transform (FFT) analysis of the whole signal. The total duration of data acquisition was not long enough to accurately capture frequencies below 10 Hz

using standard FFT analysis, preventing any strong conclusion from voltage signal about the effect of wire speed fluctuations or metal transfer. Further research using advanced signal processing techniques might be of help, and that is the motivation for including the complete raw data acquired in SOM5. The peaks occurring at 8000 Hz and above are most likely due to the electrical circuits and not to physical phenomena during metal transfer, since both droplet transfer rate and the fundamental mode of oscillation of the droplets are well below 8000 Hz. Fast phenomena such as little bursts in the melt do not occur with enough regularity as to create a sharp peak at 8000 Hz either.

Between 30 and 3000 Hz, the FFT spectrum resembles a $1/f$ pink noise, typical of many natural phenomena. In pink noise, there is no dominant frequency, but instead random fluctuations of amplitude proportional to the reciprocal of their frequency. In this case, all octaves contain the same amount of energy, but no other meaningful statement can be drawn from it at this point. If separate FFT analysis is performed independently for regions A, B, and C, they show the same type of pink noise for all three regions, and they are undistinguishable from each other.

Atmosphere in the Cavity

Following Ref. 8, a flow of gas was used in an attempt to prevent the flux cavity from collapsing because of the presence of the tunnel. Video SOM1 shows such strong ejection from both sides of the tunnel that it is unlikely any gas comes from the tunnel into the flux cavity or that the cavity will collapse because of a lack of internal pressure. No experiments were attempted without gas, but different gases were tested in an attempt to identify possible contamination in the atmosphere of the flux cavity that might affect the metal transfer and make the observations not representative.

Experiment 15 was carried out with the same parameters as Experiment 5, but using Ne instead of CO_2 as the gas injected into the tunnel. The rationale for this experiment is that Ne has very distinctive peaks in its spectrum; therefore, if any external gas entered

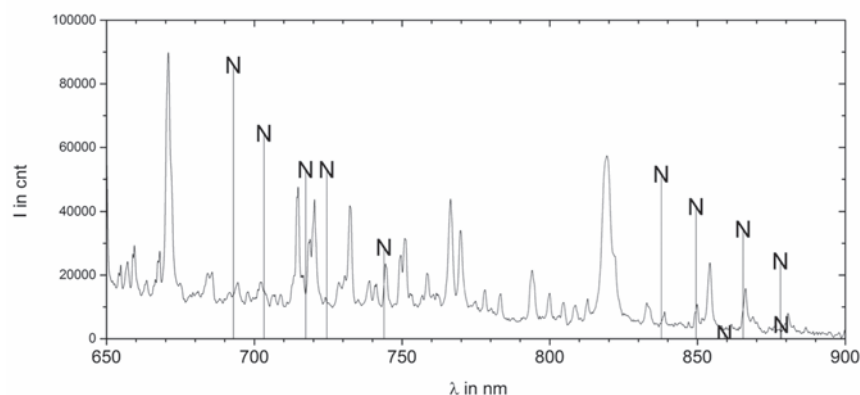


Fig. 6 — Spectrum of Experiment 15. Vertical lines indicated as “N” represent the location of spectral lines to be expected from Ne.

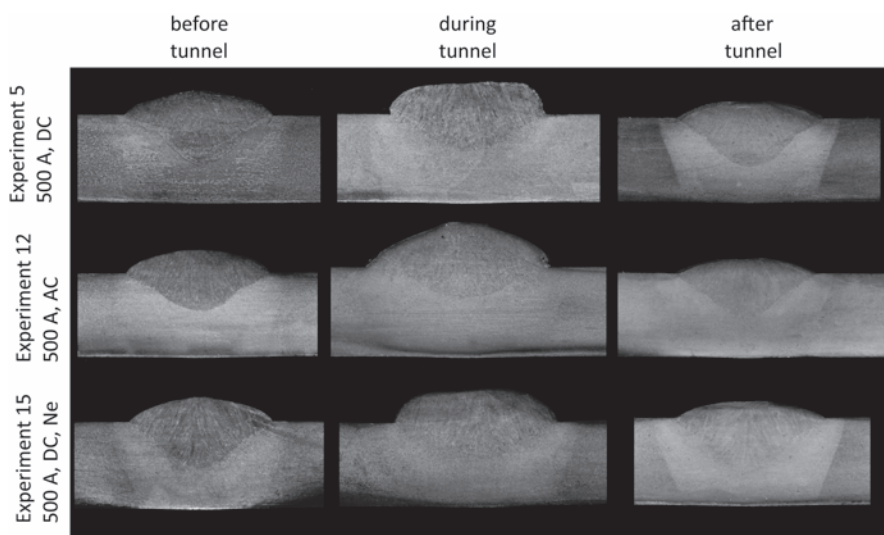


Fig. 7 — Cross sections before, during, and after the tunnel. All photos have the same magnification. For reference of scale, the average plate thickness is 9.45 mm.

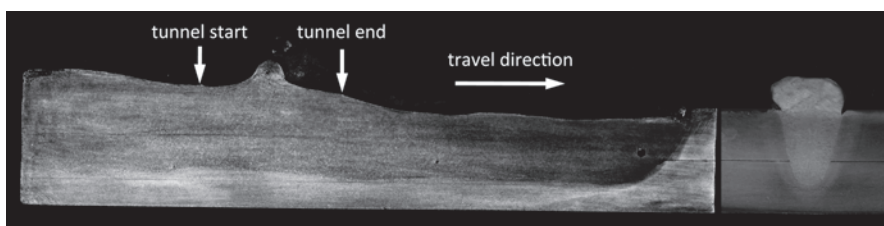


Fig. 8 — Longitudinal and cross section images of Experiment 10 indicating the location of the tunnel. It can be seen how at the beginning of the tunnel penetration is slightly reduced. Both views have the same magnification. For reference of scale, the thickness of the substrate (two plates) is 18.82 mm.

the tunnel, it would carry Ne and would be detected. Figure 6 illustrates the spectrum collected from light coming from the cavity. In this figure, the vertical lines indicated as “N” represent the location of spectral lines to be expected from Ne. It is evident there are no peaks in the spectrum matching

the location of Ne lines, suggesting that the injection of gas proposed in Ref. 8 does not affect the atmosphere inside the flux cavity, and an external injection of gas might not be necessary to keep the weld cavity open.

Video SOM6 corresponds to Experiment 15, executed with the same pa-

rameters as Experiment 5, but using Ne instead of CO₂. Within the chaotic behavior observed, there is no significant difference in the metal transfer mode between the videos of Experiments 5 and 15. Frames 2430 to 2500 show one of many occurrences of a bright swirl on the right third of the screen. These swirls are not observed when Ar or CO₂ were used as the gas. It is possible that some residual neon is trapped in the cavity. The lack of spectral lines suggests this Ne is not entrained in the arc. Another interesting feature of the Experiment 15 video is to see the flux falling onto the melting electrode in Frames 5700 to 6200.

The absence of neon lines in spectrometry is a compelling argument that the atmosphere inside the cavity is representative of that when there is no tunnel. More research needs to be performed, however, to ensure this is true. Potential sources of error include the possibility that the intensity of unfiltered light that reaches the spectrometer masks potential neon emissions from the arc.

Analysis of Weld Beads

For the four experiments considered in this paper, sections were taken to measure the perturbations introduced by the tunnel in the weld bead. For Experiments 5, 12, and 15, cross sections were taken before, in the middle, and after the tunnel. For Experiment 10, a longitudinal cross section along the centerline was taken to capture the effect of different metal transfer modes as the electrode cuts the tunnel walls.

Figure 7 compares the cross sections obtained, and Table 2 summarizes the measurements taken. Plate thickness was measured with a micrometer with 0.001-mm readout resolution, and width, depth, and reinforcement were measured counting pixels in images of 300 dots per inch resolution. The accuracy of this measurement is of the order of 0.1 mm.

Table 2 shows that when comparing the portions of the weld during the tunnel or outside, the beads tend to be slightly wider during the tunnel (by approximately 4 mm), and penetration tends to be shallower (by approximately 1 mm). Figure 7 also shows slightly different shapes for the weld reinforce-

ment inside and outside the tunnel. The presence of a tunnel has a measurable effect on the weld. One possible reason for the different widths and penetrations measured during the tunnel is that the weld cavity might partially collapse because of the lower gas pressure caused by the tunnel being open to the atmosphere. Future research should confirm whether the metal transfer mode observed in the tunnel is representative of the metal transfer mode during normal welding.

Analysis of the cross sections also shows that outside the tunnel, bead width and penetration for Experiments 5 and 15 (done with the same parameters but different gas in the tunnel) are very similar, supporting the hypothesis that the gas aimed at one end of the tunnel did not influence the process. Experiment 12, performed with the same current as Experiment 5, but with 25% of the time in electrode negative, shows a reduction of penetration of almost 1.3 mm, as expected from a reduction of time in which the substrate acts as a cathode.

Figure 8 shows the longitudinal section at the sagittal plane and a cross section before the tunnel of the weld bead in Experiment 10 (performed at 1000 A, DC). For this experiment, a high value of depth to width ratio can be appreciated on the cross section, and there is an increase in penetration (measured before the tunnel) of almost 140% compared to Experiment 5. This behavior is consistent with a change in penetration mechanism from one involving convective flows under the arc (typical of globular transfer) to one involving a gouging action of the arc (typical of high-current arc welding). Figure 8 indicates the location of the tunnel, with a slight decrease in penetration at the beginning of the tunnel. This is consistent with the globular mode of metal transfer observed in the video (SOM4) when the electrode is cutting into the tunnel, and later transitions to a buried arc with likely an arc-gouging penetration mechanism. The small protuberance observed on the surface of the weld in the middle of the tunnel is an artifact of this particular section.

Because for Experiment 10 the sectioning was done longitudinally, only a cross section before the tunnel was

available (shown on the right of Fig. 8). Measures of depth are unreliable in longitudinal welds because they are affected by small departures from the true centerline, and measures of width are not possible; in consequence, Table 2 includes only “before the tunnel” measurements.

In all experiments, the weld was stopped shortly after the exit of the tunnel (approximately 60 mm or 5 s), while the trailing tail of the weld pool was still under the tunnel, affecting the measurements of cross sections under and after the tunnel because they did not reach steady state before they solidified.

Discussion

The importance of observing metal transfer in SAW cannot be overstated. The technique presented here succeeded in making high-speed videos of SAW by using a tunnel, which is not part of a standard SAW process. The most important question to address is then, “is the metal transfer observed in the videos representative of SAW without a tunnel?” The final answer to this question cannot be settled in a single paper and requires the involvement of many researchers challenging the methodology from different points of view. In this first work, the validity of this methodology was addressed using three different approaches: analysis of the electrical signal, spectroscopy of the gas in the weld cavity, and analysis of weld cross sections.

The analysis of electrical signal using FFT did not show an obvious difference in the spectrum before, during, and after the tunnel. This supports the methodology proposed. This test, however, is not exhaustive. The minimum frequency achievable in the analysis was still too high to detect any traces of the metal transfer, and visual inspection of Fig. 4 shows that at least for Experiment 5, the voltage oscillations related to wire feed speed are not as clear while traversing the tunnel as they are before or after the tunnel. The raw data acquisition of voltage, current, and wire feed speed of the experiments discussed here is included in Spreadsheet SOM5 for follow-up analysis by other researchers interested in this field.

Analysis of the atmosphere in the

cavity was performed by injecting neon into the tunnel and performing spectroscopy of the resulting plasma. Figure 6 shows that the resulting spectrum does not include any peak for neon, suggesting that the gases generated by the fluxes pushed away all other gases in the tunnel. Strong jets were always observed ejecting from both ends of the tunnel as seen in Video SOM1, likely pushing any external gases away from the cavity. The absence of neon peaks supports the methodology proposed. Although encouraging, further validation is necessary. For example, it must be determined with certainty that the peaks were absent and not just masked under the strong light of the rest of the spectrum. In addition to the plasma, the role of the molten flux in conducting electricity between the wire and the base plate is unknown. If conduction through molten flux is important, the effect of disturbing the flux with a tunnel, as seen should be quantified in future work.

Analysis of the cross sections shows a small, but measurable, difference in weld width and penetration under the tunnel. In addition, visual inspection of the beads after each experiment indicated the slag did not peel off easily from the weld performed under the tunnel. Also, at 1000 A, the mode of metal transfer seems to be affected while cutting through the tunnel vertical walls. Although all these differences seem to be small, further research is needed to prove they are indeed negligible.

Some experimental aspects can be improved in future research. A rectangular tunnel cross section might be a better choice for the rectangular shape of the videos. Using very thin, nonconducting materials for the tunnel (or electrically insulating a metallic tunnel) might avoid the problem of stray arcs between the electrode and the tunnel. The challenge in this case will be to locally melt the tunnel before it contacts the wire. The injection of gas into the tunnel seems to have little to no effect on the arc, but when gas is not injected, stray flux powders often block the view of the camera when the arc starts to cut through the tunnel.

Conclusions

High-speed videos of metal transfer

in submerged arc welding have been captured and are published for the first time in almost 40 years. These videos, together with accompanying data acquisition, indicate the absence of short circuit metal transfer in all cases observed. At 500 A a very chaotic, nonaxial globular metal transfer involving frequent explosions and bursts was observed for both AC and DC polarities. The droplet size is so large that capillary forces are not enough to maintain it spherical. Surface tension forces are expected to result in low droplet oscillation frequencies (approximately 86 Hz for Experiment 5), much slower than the time scale of the events observed in the videos. The size of perturbations observed during metal transfer are of the same scale as the arc length. During the EN cycle in AC, the cathode spot causes significant deformation to the droplet before detachment. A droplet detachment frequency of approximately 9 Hz was observed at 500-A DCEP, and 13 Hz at 500-A AC. At 1000-A DCEP, a tapering electrode tip with a buried arc ejected a molten tail through a mechanism resembling an electromagnetic kink instability. Streaming spray transfer like in GMAW was not observed, but cannot be discarded for parameters or fluxes different than those tested here. The spatter at 500 A and the ejections at 1000 A were observed to be retained by the walls of the molten flux cavity, and are expected to slide down into the weld pool.

Analysis of the voltage signal indicates a $1/f$ pink noise without any indication of the events observed in the videos; it is likely the large size of the perturbations observed during metal transfer masks detachment or oscillation events. The lower limit of analysis (10 Hz) was not low enough to capture the variations in wire feed speed (4.7 Hz) or the frequency of droplet detachment measured from videos.

Spectrometry of the arc in the weld cavity was performed and no obvious signs of external gas entrainment were detected.

Analysis of the weld cross sections show a slight increase in width and a slight decrease in depth for the weld performed in the tunnel (where videos were taken) compared to outside the tunnel. A significant increase in penetration is observed at 1000 A, which is

consistent with the gouging region penetration mode observed in the videos.

The analysis performed suggests the metal transfer in SAW observed with the use of a properly set up tunnel is representative of metal transfer during normal operation. Further research is needed to confirm the usefulness of the technique presented here, and to invite and assist future researchers in this area, the raw data is uploaded as supporting online material listed in the references section.

If indeed successful, this technique opens the door for high-speed video analysis of metal transfer in SAW much like it has done for GMAW. Modern SAW machines have hardware capable of producing complex waveforms, but in the absence of high-speed video (and because the electrical signal shows no traces of metal transfer), there was no way of analyzing the effect of waveform shape on metal transfer. Tailored SAW waveforms designed for particular applications, wires, and fluxes might be commercially available in the near future.

Acknowledgments

The authors would like to thank Lincoln Electric for supplying the welding equipment and donating the consumables; Praxair for donating the neon used; Goetz Dapp for formatting the videos uploaded; Vivek Sengupta for the metallographic analysis and very insightful comments on the manuscript; Gentry Wood and Nairn Barnes for assistance with experiments; Ying Wang for assistance with data analysis; Johannes Schäfer for helpful comments on literature; and NSERC for partial funding of this project.

References

- Lancaster, J. F. 1986. *The Physics of Welding*. Pergamon Press, 2nd edition.
- Cho, D.-W., Song, W.-H., Cho, M.-H., and Na, S.-J. 2013. Analysis of submerged arc welding process by three-dimensional computational fluid dynamics simulations. *Journal of Materials Processing Technology* 213(12): 2278–2291.
- Tanaka, M., Shigeta, M., Miyasaka, F., and Kasano, K. 2015. A simplified numerical model of submerged arc welding. International Institute of Welding, IIW Doc. 212-1376-15.
- Pokhodnya, I. E., and Kostenko, B. A. 1965. Fusion of electrode metal and its interaction with the slag during submerged arc welding. *Autom. Weld.* 18.
- Eichhorn, F., and Diltthey, V. 1971. High-speed x-ray photography for submerged arc welding. *Metal Construction and British Welding Journal* 3(12): 453–456.
- Rokhlin, S. I., and Guu, A. C. 1990. Computerized radiographic sensing and control of an arc welding process. *Welding Journal* 69(3): 83-s to 97-s.
- Tybus, G. 1957. Farbige Zeitlupenaufnahmen zur Beobachtung des Schweißbades beim UP-Schweiß. *Schweisstechnik* (3): 68–71.
- Franz, U. 1965. Vorgänge in der Kavertube beim UP-Schweiß. Dipl.-Ing. dissertation. Fakultät für Maschinenbau, Technischen Hochschule Otto von Guericke.
- Lancaster, J. F. 1987. The physics of fusion-welding. Part 2: Mass-transfer and heat-flow. *IEE Proceedings-B Electric Power Applications* 134(6): 297–316.
- Van Adrichem, J. T. 1966. Metal transfer in submerged arc welding. International Institute of Welding, IIW Document 212-78-66.
- Gupta, P. C., Rehfeldt, D., and Erdmann-Jesnitzer, F. 1976. Influence of current pulses during submerged arc-welding. *Welding Journal* 55(11): 377-s to 380-s.
- Mendez, P. F., Goett, G., and Guest, S. D. 2014. High speed video of metal transfer in submerged arc welding. International Institute of Welding, IIW Doc. 212-1345-14.
- Reisgen, U., Willms, K., Sharma, R., and Schäfer, J. 2015. Diagnostic process analysis of the submerged-arc by welding high-strength fine-grained structural steels. International Institute of Welding, IIW Doc. XII-2205-15.
- http://www.ualberta.ca/~ccwj/Publications/WJ_HSV_SAW/
SOM1: ccwj_000015.001.mp4
SOM2: ccwj_000015.002.mp4
SOM3: ccwj_000015.003.mp4
SOM4: ccwj_000015.004.mp4
SOM5: ccwj_000015.005.xlsx
SOM6: ccwj_000015.006.mp4